Heliyon 10 (2024) e32228

Contents lists available at ScienceDirect

Heliyon

journal homepage: www.cell.com/heliyon

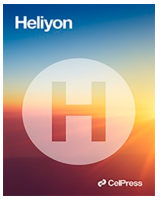

Research article

A rapid protocol for synthesis of chitosan nanoparticles with ideal physicochemical features

Hamed Dadashi [a,b,c], Somayeh Vandghanooni [d], Shahrbanoo Karamnejad-Faragheh [a], Alireza Karimian-Shaddel [a], Morteza Eskandani [a,*], Rana Jahanban-Esfahlan [b,**]

[a] Research Center for Pharmaceutical Nanotechnology, Biomedicine Institute, Tabriz University of Medical Sciences, Tabriz, Iran
[b] Department of Medical Biotechnology, Faculty of Advanced Medical Sciences, Tabriz University of Medical Sciences, Tabriz, Iran
[c] Drug Applied Research Center, Faculty of Advanced Medical Sciences, Tabriz University of Medical Sciences, Tabriz, Iran
[d] Hematology and Oncology Research Center, Tabriz university of Medical Sciences, Tabriz, Iran

ARTICLE INFO

Keywords:
Cs nanoparticles
Synthesis
Particle size
Zeta potential
Drug delivery system
Biocompatibility
Stability

ABSTRACT

In this research, an innovative protocol is introduced to address crucial deficiencies in the formulation of chitosan nanoparticles (Cs NPs). While NPs show potential in drug delivery systems (DDSs), their application in the clinic is hindered by various drawbacks, such as toxicity, high material costs, and time-consuming and challenging preparation procedures. Within polymer-based NPs, Cs is a plentiful natural substance derived from the deacetylation of chitin, which can be sourced from the shells of shrimp or crab. Cs NPs can be formulated using the ionic gelation technique, which involves the use of a negatively charged agent, such as tripolyphosphate (TPP), as a crosslinking agent. Even though Cs is a cost-effective and biocompatible material, the formulation of Cs NPs with the correct size and surface electrical charge (zeta potential) presents a persistent challenge. In this study, various techniques were employed to analyze the prepared Cs NPs. The size and surface charge of the NPs were evaluated using dynamic light scattering (DLS). Morphological analysis was conducted using field emission-scanning electron microscopy (FE-SEM). The chemical composition and formation of Cs NPs were investigated using Fourier transform infrared (FTIR). The stability analysis was confirmed through X-ray diffraction (XRD) analysis. Lastly, the biocompatibility of the NPs was assessed through cell cytotoxicity evaluation using the MTT assay. Moreover, here, 11 formulations with different parameters such as reaction pH, Cs:TPP ratio, type of Cs/TPP, and ultrasonication procedure were prepared. Formulation 11 was chosen as the optimized formulation based on its high stability of more than three months, biocompatibility, nanosize of 75.6 ± 18.24 nm, and zeta potential of $+26.7$ mV. To conclude, the method described here is easy and reproducible and can be used for facile preparation of Cs NPs with desirable physicochemical characteristics and engineering ideal platforms for drug delivery purposes.

* Corresponding author. Research Center for Pharmaceutical Nanotechnology, Tabriz University of Medical Sciences, Tabriz, Iran.
** Corresponding author.
E-mail addresses: eskandanim@tbzmed.ac.ir (M. Eskandani), jahanbanr@tbzmed.ac.ir (R. Jahanban-Esfahlan).

https://doi.org/10.1016/j.heliyon.2024.e32228
Received 28 August 2023; Received in revised form 29 May 2024; Accepted 30 May 2024
Available online 3 June 2024

1. Introduction

Nanobiotechnology plays a significant role in designing novel therapeutic strategies that are more effective and show fewer side effects compared to conventional therapies. For years, attempts have been focused on the design and formulation of better pharmaceutical products for a variety of health conditions, including neurological issues, heart diseases, metabolic disorders, infectious conditions, diabetes, and cancer. In this regard, one of the most outstanding fields for formulating nanocarriers is nano drug delivery systems (NDDSs) [1]. Examples of the most common NDDSs comprise metallic (e.g., silver, gold, and iron, etc.) [2–4], carbon-based [5,6], quantum dot [7], synthetic polymers (e.g., poly(lactic-*co*-glycolic acid) (PLGA) [8–12]), natural polymers like chitosan (Cs) [13–15], β-cyclodextrin [16], gelatin [17], bovine serum albumin [18], and lipid-based [19] (e.g., liposomes [20,21] and solid lipid nanoparticles (SLNs) [22,23]), nanoparticles (NPs), among others. Each of these NPs shows considerable characteristics as NDDSs [24], while they may own tangible weaknesses like toxicity [25], high material prices, and hard and sophisticated preparation procedures, which may be addressed by considering or altering some important factors. For instance, while natural compounds are better candidates to reduce the toxicity issue of NPs [26], their stability can be compromised by factors such as the level of crystallinity, wettability, and sensitivity to heat [27,28]. Among natural biomaterials, Cs is a non-toxic, natural polymer that can address many challenges regarding suitable NP preparation. It is also an inexpensive material and can be easily found and purchased [15]. Cs (poly-(D) glucosamine) is a deacetylated extract of chitin, which can be obtained from the shell of shrimp or crab. This compound has several NH_2 functional groups that endow this linear polymer with a high positive electric charge, which can be useful for further modifications (Fig. 1a). There are several physical or chemical methods for the preparation of Cs NPs or nanogels. One simple physical method is ionic gelation [29], in which a negatively charged compound, like tripolyphosphate (TPP) or positively charged calcium chloride, is used as a crosslinker agent to form polymeric networks of Cs [14] or alginate NPs [30], respectively (Fig. 1b). Importantly, due to the natural origin of Cs, the synthesized NPs are endowed with biocompatibility, which plays a critical role in pharmaceutical nanotechnology and provides a safer drug delivery system. Cs NPs have found utility in various fields such as agriculture [31], food industry [32], environmental remediation [33], gene therapy [34], and tissue engineering [35]. This adaptability makes them a versatile and adaptable tool. Considering the favorable features of Cs for NDDSs, several challenges regarding preparing suitable NPs still need to be addressed. For example, the synthesis process of these NPs is very sensitive to pH, temperature, concentration of used materials, and even the length of the preparation procedure. As a result, in practice, it is difficult to prepare Cs NPs with ideal nanosize and surface charge that assure optimum bio-distribution, circulation, localization, and cellular uptake [36–40]. This research specifically addresses the difficulties associated with regulating the size of NPs, manipulating their surface charge, and managing the sensitivity of the synthesis process to different factors. Likewise, in this study, Cs NPs are selected due to their outstanding advantages, such as non-toxicity, affordability, and versatility. The main objective of this study is to present an easy way to synthesize Cs NPs with the desired physicochemical properties. Here, two different types of Cs (based on molecular weight that, according to experience, can directly affect the nanosize) and TPP (based on producer company) are used, and different formulations with various results are described. In addition, this study investigates the role of pH, Cs:TPP amount ratio, ultrasonication time and amplitude, and the type of

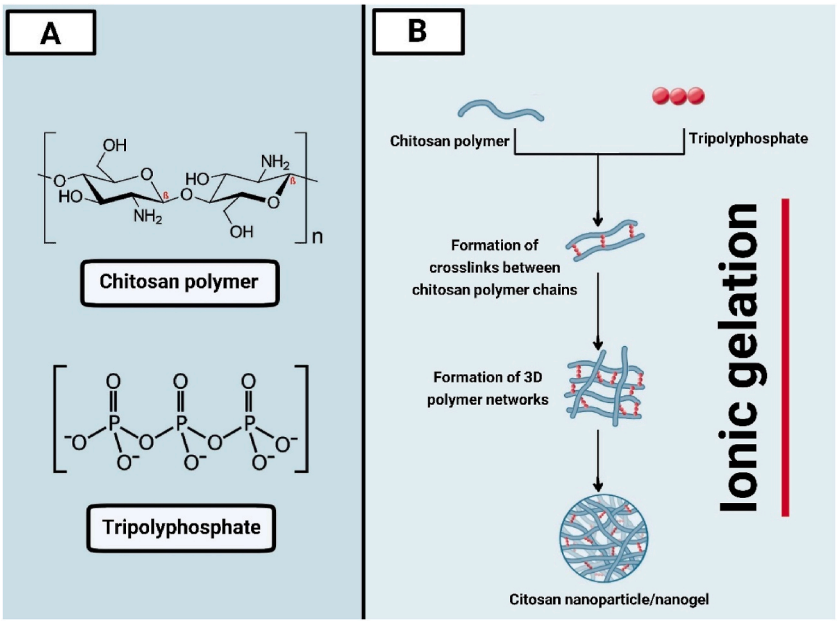

Fig. 1. Molecular structure of Cs polymer and tripolyphosphate (**A**) and schematic illustration of the ionic gelation method regarding Cs NPs formation (**B**). Cs polymer contains NH_2 groups, which cause a positive charge, while TPP, due to its phosphate groups, is an anionic compound. The addition of TPP to Cs solution causes the formation of crosslinks between the NH_2 groups of the Cs polymer, which leads to Cs NPs formation.

used materials in influencing the size and the surface charge of synthesized Cs NPs. Here, Cs NPs regarding the chosen formulation were synthesized with a size less than 100 nm and a proper surface positive charge, which, according to the points highlighted in the previous paragraph, makes them promising and biocompatible nanocarriers with an optimal cellular uptake.

2. Materials and methods

2.1. Materials

Two different Cs polymers with molecular weights (MW) of ~50–190 and ~50 kDa (Sigma Aldrich, St. Louis, MO, USA) and two types of TPP, one from Sigma Aldrich and one from Merk Millipore (Burlington, MA, USA), were purchased. Phosphate buffered saline (PBS), 3-(4,5-dimethyl-2-thiazolyl)-2,5-diphenyl-2Htetrazolium bromide (MTT), and Trypsin-EDTA were obtained from Sigma Aldrich. The sources of other used materials were as follows: RPMI1640 and FBS (Gibco life technologies, Waltham, MA, USA) and penicillin/streptomycin (ScienCell, Carlsbad, CA, USA). Sodium hydroxide (NaOH), hydrochloric acid (HCl), acetic acid (AA), and other reagents and solvents used in this work were analytical grade and were obtained from Merck Millipore.

2.2. Preparation of Cs NPs

First, the TPP solutions were prepared with a certain concentration and pH (pH adjustment was done using 1 M NaOH and HCL solutions utilizing a Metrohm 827 digital pH meter (Herisau, Switzerland)) and kept at room temperature. More details and the effects of differing factors such as pH and concentration are listed in Table 1. Then, a certain amount of Cs (equal to the concentration of TPP) was added to a beaker containing 8 mL of distilled water on a magnetic stirrer. After, the beakers were incubated at 35–40 °C for 10 min at a slow stirring rate. To dissolve Cs, AA (1 % v/v) was added to the solution. After, the solution was mixed at the maximum rate on a magnetic stirrer to ensure the complete dissolution of Cs powder. Then a clear Cs solution was centrifuged at 12,000×*g* at 10 °C for 10 min to remove unwanted ingredients. After centrifugation, the supernatant must be completely collected and adjusted to a certain pH. It should be noted that the concentration and pH of TPP and Cs solutions were equal for each formulation.

After the pH adjustment of the Cs solution, the solution-containing beaker was placed on ice. Before adding TPP, an insulin syringe needle was connected to a 5 mL syringe. Then a certain volume of TPP solution was added to the syringe in the absence of the plunger. TPP should be added to the Cs solution while the fall of the drops occurs due to gravity (see Fig. 2). It is important to add TPP drops to the Cs solution while it is being stirred at maximum intensity.

After the addition of TPP, the solution was poured into a 15 mL falcon tube and subjected to ultrasonication using a Sonopulse ultrasonicator (Bendelin, Berlin, Germany). When the ultrasonication was done, the Cs NP suspensions were placed into glass vials and kept at 4 °C.

2.3. Characterization of Cs NPs

2.3.1. NP size and surface electric charge

The size distribution and surface charge (zeta potential) were measured at pH 7.0 using a Malvern zetasizer 3000 HS (Worcestershire, UK). The system settings for the size measurement were as follows: measurement position (mm): 5.5, duration used (s): 4, attenuator: 6. Additionally, the settings for zeta potential measurement were: measurement position (mm): 2, zeta runs: 12, attenuator: 7. Also in the equipment setting, the dielectric constant was 78.5 and the field strength was 5 kV/m. Samples were diluted in distilled water (1:10) and tubes kept on ice until the measurement was performed immediately.

Table 1
Details of the formulations studied for synthesis of Cs NPs.

Formulation number	Type of Cs	Type of TPP	TPP:Cs Ratio	Con (% w/v)	pH	Ultrasonication procedure
1	~160 kDa	SA	1:3.5	0.7	5	2.5 min 60 % Am + 1min 80 % Am
2	~160 kDa	SA	1:3.5	0.5	5	2.5 min 60 % Am + 1min 80 % Am
3	~160 kDa	SA	1:3	0.5	4.5	2.5 min 60 % Am + 1min 80 % Am
4	~160 kDa	MM	1:3.5	0.5	5	2.5 min 60 % Am + 1min 80 % Am
5	~160 kDa	SA	1:3.5	0.25	5	2.5 min 60 % Am + 1min 80 % Am
6	~160 kDa	MM	1:4	0.25	5	2.5 min 60 % Am + 30s 80 % Am
7	~160 kDa	SA	1:4	0.25	5	2.5 min 60 % Am + 20s 80 % Am
8	~160 kDa	SA	1:4	0.25	5	2.5 min 60 % Am + 30s 80 % Am
9	~50 kDa	MM	1:4	0.25	5	2.5 min 60 % Am
10	~50 kDa	MM	1:4	0.25	5	2.5 min 60 % Am + 30s 80%Am
11	~50 kDa	MM	1:4	0.25	5	2.5 min 60 % Am + 30s 80%Am***

Am: Amplitude, Con: Concentration, Cs: Cs, MM: Merk Millipore, SA: Sigma Aldrich. The exact settings of ultrasonication plans are listed briefly in the related column. For example, formulation number 1 has undergone 2.5 min of ultrasonication at 60 % amplitude and 1 min at 80 % amplitude. The ultrasonication power and frequency may be converted and/or adjusted according to the type of ultrasonicator used. ***: Two identical aliquots were prepared from the suspension after ultrasonication with 60 % amplitude, and one of them was sonicated with 80 % amplitude for 30 s.

Fig. 2. Photo of the process of the dropwise addition of TPP solution to Cs solution. The dropwise addition of TPP solution with the described syringe to ice-cold Cs solution presents a controlled and slow mixing procedure that leads to the repeatability of a certain formulation.

2.3.2. Morphological analysis

Morphological analysis was performed using field emission scanning electron microscopy (FE-SEM) (MV2300, Brno, Czech Republic). To prepare the samples, the NP suspension was diluted in distilled water, and a thin, air-dried layer was prepared on a slide for each sample [41]. The magnification and the settings are presented in regarded to micrographs in Fig. 4.

2.3.3. Chemical composition analysis

Chemical composition analysis was performed utilizing a Fourier transform infrared (FTIR) spectrophotometer (Bruker, Germany). The scanned wavenumber area was 400–4000 cm^{-1}, the resolution was 4 cm^{-1}, the sample scan time was 16 scans, and the background scan time was 16 scans. The prepared samples were the Cs solution and the suspension of Cs NPs. The sample of NPs was prepared by centrifugation at 12,000×*g* at 10 °C for 30 min, twice, and the pellet was used for analysis.

2.3.4. Stability test

Formulation 11 was selected as the preferred synthesis option and stored at 4 °C and protected from light. After three months at 4 °C, size, zeta potential, and crystal analysis were performed [42].

2.3.5. X-ray diffraction (XRD) analysis

The crystal examination was carried out for both the fresh synthesis and the one stored for three months. This analysis was performed using a Tongda TD-3700 x ray diffractometer (Dandong, China) at $2\theta = 10°–60°$. The samples were prepared as thin coats of air-dried synthesis solutions on slides (a thin coat).

The analysis settings were as follows: scan rate: 0.02°/0.5 s, step size: 0.02°, time per step: 0.5 s, Anode (target material): copper, wavelength of kalpha: 1.5406 Å, voltage: 30 KV, current: 20 mA.

2.4. Biocompatibility test

2.4.1. Cell culture

The mouse fibroblast NIH-3T3 cells were used for the biocompatibility test. The culture medium was RPMI, containing 10 % FBS and 1 % penicillin/streptomycin, and cells were cultured in T25 cell culture flasks at 37 °C and 5 % CO_2.

2.4.2. Cell cytotoxicity assessment

First, NIH-3T3 cells (passage number 4) were seeded on a 96-well cell culture plate (10,000 cells per well), while the remaining wells were filled with PBS. The plate was kept in a cell culture incubator for 24 h for cell attachment. Then, the media was removed, and 6 wells were treated with fresh media (negative control), 6 wells with 5 % dimethyl sulfoxide (DMSO)-containing media (positive control), and other wells were treated with 10, 20, 50, 140, 170, and 200 μg/mL Cs NP-containing culture medium (6 wells for each treatment) [43]. After 48 h of treatment, the media was removed and replaced with MTT-containing media (100 μg/well) without washing with PBS and incubated for 4 h. Then, the media was removed and replaced with DMSO, and the plate was analyzed using a RayBiotech Stat Fax 4200 ELISA reader (Norcross, GA, USA), and absorbance was measured at 570 nm.

2.5. Statistical analysis

All procedures presented here are repeated at least three times. Data related to the NP size and the surface charge are expressed as mean ± SD. All quantitative results were analyzed using GraphPad Prism software (v9.5.1) (San Diego, CA, USA) with one-way ANOVA Followed by the Tukey test, and the significance threshold was $P < 0.05$.

3. Results

3.1. Particle size and zeta potential

The results of particle size, zeta potential, and polydispersity index (PDI) for various formulations of Cs NPs are listed in Table 2. Additionally, Fig. 3 presents a comparative analysis of size and zeta potential among formulations 1 (Fig. 3a & e), 4 (Fig. 3b & f), 10 (Fig. 3c & g), and 11 (Fig. 3d & h).The largest particle size belongs to formulation 1 (451.8 ± 193.8 nm) (see Fig. 3a), while the smallest NPs are obtained by formulation 11 (75.6 ± 18.24 nm) (see Fig. 3d). In addition, formulation 3 had the highest zeta potential, and formulation 7 had the lowest, while the zeta potential of other formulations ranged from 13.8 mV to 37.0 mV. Also, in order to report reliable results, each formulation was analyzed three times. Formulation 11 has been selected for further tests because to its smallest mean size and appropriate zeta potential. Similarly, the formulation that has the shortest size and appropriate zeta potential may demonstrate superior *in vivo* performance in comparison to the other created formulations. The statistical data comparing formulation 11 with other formulations are displayed inTables 3 and 4, presenting differences in size and zeta potential, respectively.

3.2. Morphological analysis

For morphological characterization of Cs NPs, FE-SEM micrograph acquisition was accomplished for formulations 1, 10, and 11 (Fig. 4). NPs of formulation 11 were selected due to their small size, formulation 1 for their big size, and formulation 10 for the different size compared to formulation 11, while their synthesis methods both shared so many similarities. All NPs exhibited a spherical morphology. Formulation 1 (Fig. 4a) exhibited larger Cs NPs with a high degree of size variation. In contrast, formulations 10 (Figs. 4b) and 11 (Fig. 4c) showed smaller particle sizes with a more consistent size distribution. This is consistent with the DLS results, which indicated that formulation 10 had an average size of 127.50 ± 86.88 nm, and formulation 11 had an average size of 75.60 ± 18.24 nm. On the other side, micrographs of formulation 11 show the smallest and most homogenous Cs NPs, in line with the data presented in Table 2.

Considering the results obtained from DLS measurement and FE-SEM, the appearance of Cs NPs (Fig. 5) is not only related to Cs concentration or NP formation but also to the size or size distribution of Cs NPs. Likewise, if the concentration of Cs and/or TPP, NP formation, NP size, or size heterogeneity increases (Fig. 5a), as a result, the turbidity of the suspension significantly increases as well. Conversely, formulations characterized by a uniform size distribution (as depicted in Fig. 5b & c) exhibit lower turbidity, regardless of the concentration of the resultant NPs.

3.3. FTIR

For chemical composition assessment, FTIR analysis was performed for Cs solution and Cs NPs suspension (Fig. 6). Regarding the spectra of Cs solution containing 1 % AA, a peak at 3450.18 is shown, and the related band represents the overlapped stretching vibration of OH and NH_2 groups and also indicates the presence of H_2O. The peak at 1637.08 might be related to $CONH_2$ groups. Peaks around the wavenumber ~1000 can be caused by anhydro glucosidic rings. Also, the peaks at 3450.18 and 1637.08 are shifted to lower sites on the x-axis (wavenumber) in the plot B, which might be a consequence of the interaction of the phosphate groups of TPP with the ammonium groups of Cs. Also, the wider peak at 3437.08 could be due to the increase in hydrogen bonds in Cs NPs. Moreover, an obvious peak at 774.31 disappears in plot A, and a peak at 896.22 appears, as well as a sharper peak at 1150.15, which could both be related to the PO_4^{-2} groups of TPP. In general, the fingerprint area and the whole spectrum patterns claim the carbohydrate structure of Cs as well as Cs NP formation.

Table 2
DLS results of different formulations of Cs NP.

Formulations number	Properties of synthesized Cs NPs		
	NP size (nm)	Zeta potential (mV)	PDI
1	451.80 ± 193.80	26.50 ± 5.71	0.36
2	275.30 ± 221.00	22.50 ± 11.80	0.548
3	267.90 ± 83.32	37.00 ± 4.84	0.236
4	191.10 ± 138.80	28.20 ± 4.82	0.33
5	319.60 ± 215.30	24.80 ± 11.60	0.305
6	86.40 ± 19.88	27.40 ± 6.07	0.386
7	221.80 ± 193.80	13.80 ± 4.70	0.376
8	194.30 ± 65.84	36.10 ± 5.22	0.275
9	158.80 ± 86.92	19.10 ± 5.61	0.438
10	127.50 ± 86.88	15.30 ± 4.49	0.542
11	75.60 ± 18.24	26.70 ± 4.52	0.397

The provided standard deviations are directly linked to the percentage of the detected particles.

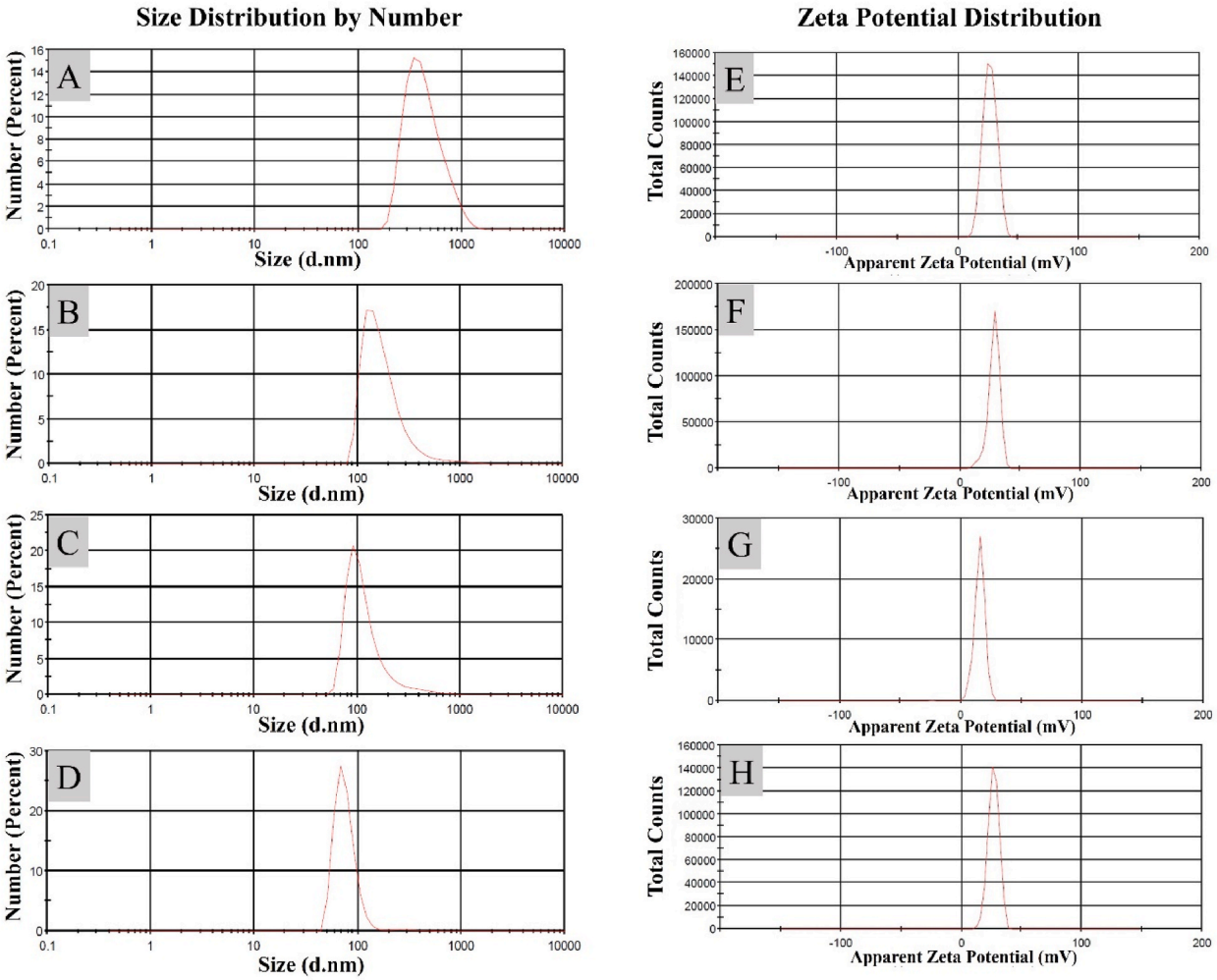

Fig. 3. Particle size and zeta potential results of formulations 1, 4, 10, and 11. **A**, **B**, **C**, and **D** correspond to the size distribution outcomes for formulations 1, 4, 10, and 11. **E**, **F**, **G**, and **H** represent the zeta potential distribution findings for formulations 1, 4, 10, and 11, respectively. The particle size peaks decrease from formulation 1 to 11, with sharp peaks indicating size uniformity. Similarly, the zeta potential results display sharp peaks, signifying consistent surface charge on the nanoparticles. Formulation 4 was selected randomly for presentation, and the results for formulation 10 were included due to the similarities in preparation methods with formulation 11.

3.4. Stability analysis

After being stored for three months, the DLS analysis of the synthesized NPs showed a size of 73.4 ± 26.24 nm and a zeta potential of 28.8 ± 4.2 mV. These measurements did not demonstrate any significant differences compared to the freshly synthesized Cs NPs. In addition, there were no instances of aggregation observed in the stored synthesis solutions after the specified time length. Also, the results of XRD (Fig. 7) show strong peaks at: A: 17.76, 26.78, 35.92, B: 17.8, 26.84, 36.2, and short peaks at A: 31.72, 45.36, B: 30.1, 31.7, and 45.52°. In line with DLS results, while some changes appeared in the spectrum of sample B, the crystal patterns of the two samples are similar, confirming the high stability of synthesized CS NPs.

3.5. Cell cytotoxicity assay

Biocompatibility of Cs NPs was assessed by MTT assay using NIH-3T3 mouse fibroblast cells, which showed no toxicity even at the highest dose of 200 μg/mL, confirming the high biocompatibility of Cs NPs upon normal cells (Fig. 8), as it increased cell survival by almost 40 % compared to the negative control. Also, no morphological changes were observed after treatment. Importantly, MTT data show that Cs NPs enhance the proliferation of NIH-3T3 cells.

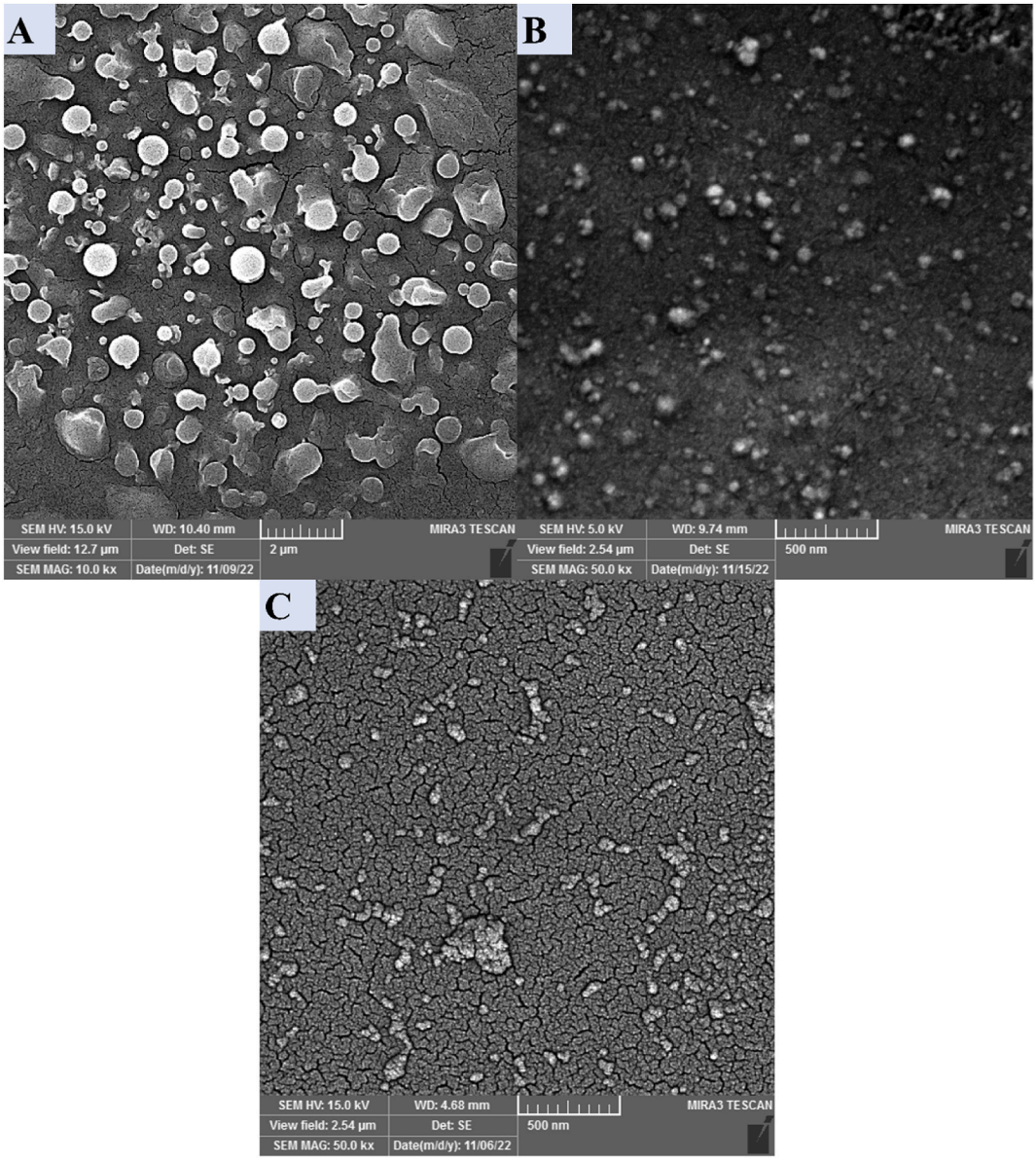

Fig. 4. FE-SEM micrographs regarding formulations 1, 10, and 11. **A** represents the micrograph of formulation 1, **B** represents formulation 10, and **C** represents formulation 11. The scale bars and imaging settings are presented for each micrograph. The FE-SEM micrograph of formulation 1 (dimension bar: 2 µm) displays non-homogenous particles with relatively large sizes. On the other hand, the micrograph of formulation 10 (dimension bar: 500 nm) shows very small sizes. Although the observed qualitative size heterogeneity is reduced, it is still similar to the micrograph of formulation 1. Furthermore, the micrograph of formulation 11 (dimension bar: 500 nm) exhibits the presence of the tiniest NPs and a satisfactory level of visual size uniformity.

4. Discussion

Nanotechnology uses a variety of NPs, and while each of these presents unique advantages as NDDSs, they also possess certain weaknesses like toxicity or size limitation, which hinder their clinical application [44–46]. Additionally, the size and surface charge of the produced NPs significantly affect their performance, biodistribution, and cellular uptake. The stability of the manufactured NPs, in addition to other indicated critical parameters, significantly contributes to the creation of a secure and efficient drug delivery system. Among polymeric nanocarriers, Cs-based NPs are attractive due to many reasons, in particular their natural, obtainable, cheap, east synthesis, and functionality [15].

Table 3
The statistical analysis report compares the size of formulation 11 with other formulations.

Formulations number	Statistical report	
	The difference of the means	P-Value/Significant summary
1	376.20	****
2	199.70	****
3	192.30	****
4	115.50	****
5	244.00	****
6	10.80	ns
7	146.20	****
8	118.70	****
9	83.20	***
10	51.90	ns

Ns: non-significant, *: $P \leq 0.05$, **: $P \leq 0.01$, $P \leq 0.001$,***: $P \leq 0.001$, ****: $P \leq 0.0001$, Ns: not significant: $P > 0.05$.

Table 4
The statistical analysis report compares the zeta potential of formulation 11 with other formulations.

11 vs.	Statistical report	
	The difference of the means	P-Value/Significance summary
1	−0.20	ns
2	−4.20	***
3	10.30	****
4	1.50	ns
5	−1.90	ns
6	0.70	ns
7	−12.90	****
8	9.40	****
9	−7.60	****
10	−11.40	****

Ns: non-significant, *: $P \leq 0.05$, **: $P \leq 0.01$, $P \leq 0.001$,***: $P \leq 0.001$, ****: $P \leq 0.0001$, ns: not significant: $P > 0.05$.

4.1. Significance of synthesis variables in NP size and surface charge

As for clinical application of NPs, physiochemical features such as size, shape, stability, and surface electric charge are indispensable for proper bio-distribution, localization, retention, and penetration *in vivo* (see our recent review [45]), thus tuning these features to engineer the ideal NP to serve as NDDS is of critical importance. When it comes to Cs NPs prepared by the ionic gelation method, engineering nanocarriers that are suitable for drug delivery is challenging. Several factors are involved in the synthesis process, such as the Cs:TPP ratio, the concentration of the materials used, type of the materials, the pH of reaction solutions, the time length of TPP addition, and the ultrasonication procedure. Though there are many protocols for the synthesis of Cs NPs, here we provide an intricate yet straightforward, expeditious, and distinctive method for reproducible synthesis of Cs NPs as an ideal NDDS for the encapsulation of a variety of bioactive materials, e.g., for cancer therapy purposes.

It is evident that the timing of adding TPP is crucial among several parameters, and a gradual and consistent addition of TPP to the Cs solution is essential for a successful synthesis in terms of physical stability and size distribution. Likewise, the type of used material is another aspect that should be considered. This study showed that the molecular weight of Cs influences the size of NPs. Another critical characteristic of NPs is their surface charge, reported as zeta potential (mV), which is controlled by three main factors including the type of material used, the TPP:Cs ratio, and the pH of the reaction. Among these, pH changes result in noticeable changes in zeta potential. For example, the pH of the reaction solution for formulation 3 was 4.5, whereas the pH in other formulations was 5. Additionally, with a TPP:Cs ratio of 1:3, the resulting zeta potential was +37 mV, highlighting the significant role of pH on the electric charge of the NP surface. Not to mention that higher amounts of TPP lead to a lower positive surface charge. Though formulations 6 and 11 exhibited satisfactory characteristics with sizes of approximately 86.4 nm and 75.6 nm, and zeta potentials of around +27.4 mV and +26.7 mV, respectively, the FE-SEM images and DLS size distribution analysis of formulation 11 (Figs. 3d and 4c) revealed that it produced the smallest and most uniform Cs nanoparticles compared to all other formulations. Moreover, considering the impact of ultrasonication on NP size, the distinction between formulations 10 and 11 lies in the approach employed. In formulation 11, following sonication at 60 % amplitude, the suspension was split into two equal aliquots, with each undergoing sonication at 80 % amplitude. The corresponding findings suggest that a reduced sample volume enhances the ultrasonication effect, consequently resulting in the reduction of NP size. Fig. 9 summarizes the significant variants that lead to Cs NPs with favorable size and zeta potential.

4.2. Stability and biocompatibility

Another important criterion for a perfect NDDS is its stability. Synthesis stability analysis was performed using the fresh samples

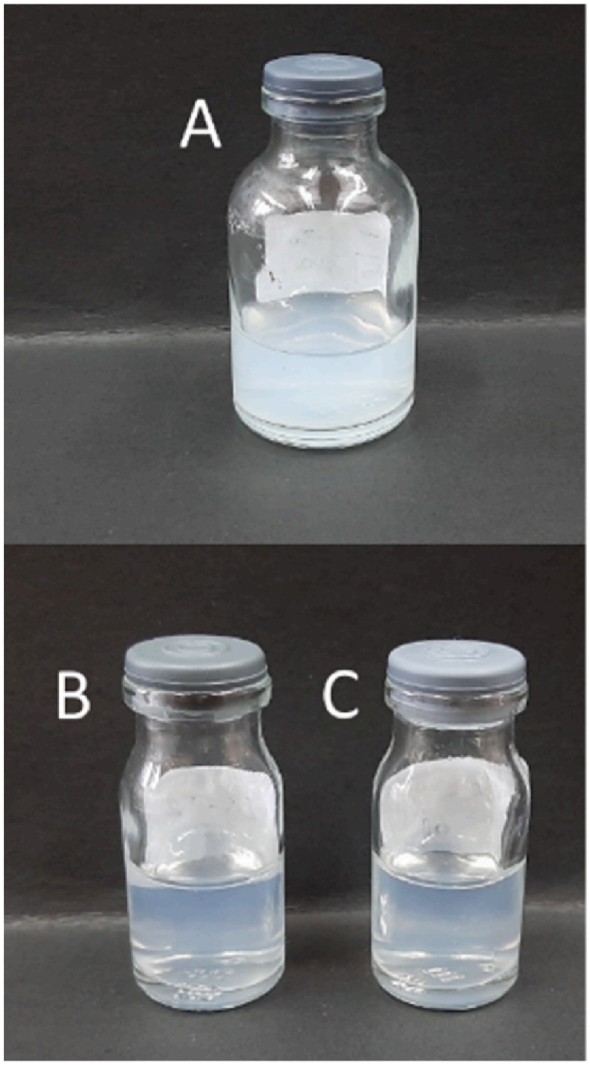

Fig. 5. Photos of the final appearance of formulations 4, 9, and 11. Formulation 4 (**A**) (concentration: 0.50 % w/v, mean size: 191.10) had high turbidity, while formulations 11 (**B**) (concentration: 0.25 % w/v, mean size: 75.60) and 9 (**C**) (concentration: 0.25 % w/v, mean size: 158.80) were associated with less turbidity.

and the samples that were stored for three months. No significant changes were observed regarding particle size or zeta potential. In addition, based on the XRD findings, it can be concluded that the synthesis remains stable for an extended period of time, which is a crucial factor for drug delivery purposes. When it comes to *in vivo* application, NP should possess a biocompatibility and non-toxicity profile with normal cells. To this end, we validated that higher doses of Cs NPs not only have no toxicity on NIH-3T3 mouse fibroblast cells, but also tend to increase cell viability. The determined non-toxicity of the studied Cs NPs highlights that they may exhibit a desired performance *in vivo*.

4.3. Comparative advantages of optimized Cs NPs

Furthermore, when examining formulation 11, as reported in this study, it exhibits distinct properties in comparison to other recent studies where researchers have utilized similar or different methodologies to prepare Cs NPs for various purposes. For instance, Fahmy et al. have used Cs NPs for ascorbic acid and oxaliplatin delivery to breast cancer cells [47]. In this work, the reported NP size and zeta potential were ~290.3 nm and ~27.6 mV, respectively. While the surface charge is similar to our candidate formulation, the size is much larger. Also, Hadidi et al. prepared Cs NPs for loading clove essential oil, and the size of the NPs was ~223.2 nm with a zeta potential of 34.5 mV [48]. In addition, Choudhary et al. reported the formulation of zinc-loaded Cs NPs to study their effect on the yield of maize crops, in which the size of the NPs was ~387.7 nm and the zeta potential was ~34 mV [49]. Moreover, Sultan et al. have developed cisplatin-loaded Cs NPs with a size of ~308.1 nm, and a zeta potential of ~30.5 mV and cisplatin-loaded Cs NPs with rituximab-coated surfaces (size: ~349.4.1 nm, zeta potential: ~26.9) to treat breast cancer cells [50]. Although these studies used the

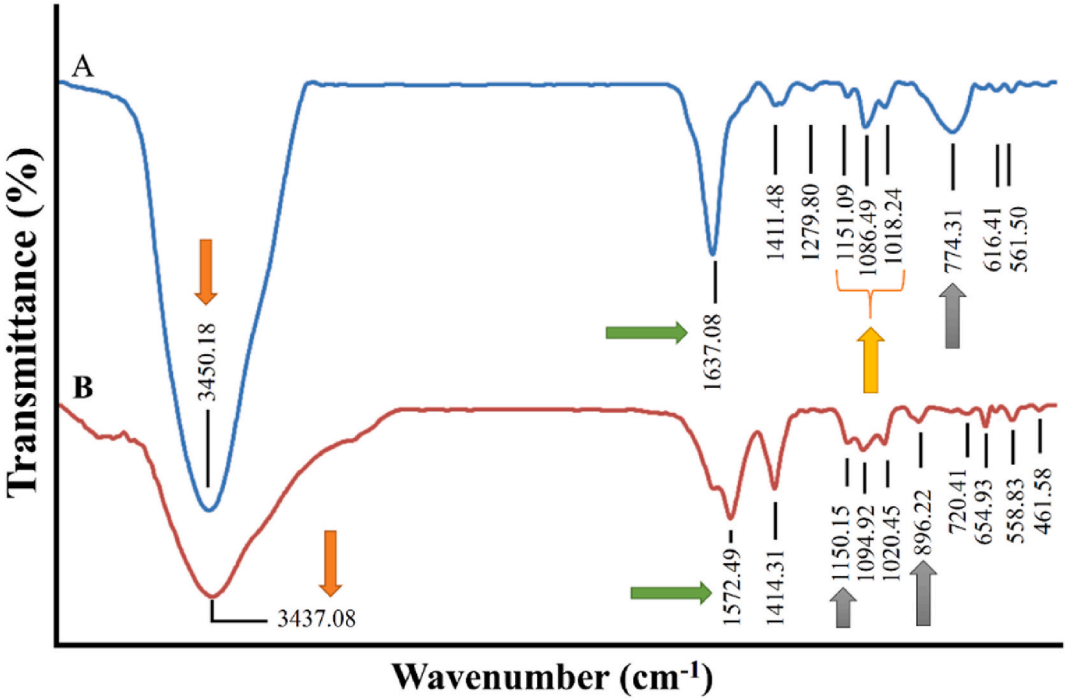

Fig. 6. FTIR spectrum of Cs solution containing 1 % AA and Cs NPs. **A** represents Cs solution, and **B** represents Cs NPs. The X axis shows wavenumber (cm^{-1}) and the Y axis shows transmittance (%). The discussed peaks and areas are displayed with arrows and their correlations are highlighted using colors. (For interpretation of the references to color in this figure legend, the reader is referred to the Web version of this article.)

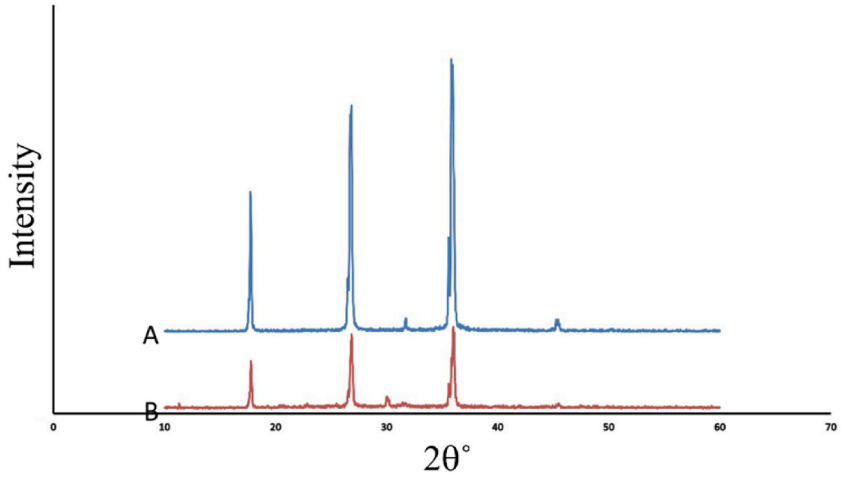

Fig. 7. XRD spectra of Cs NPs. This figure displays the XRD findings of the freshly prepared NP suspension (**A**) and the NP suspension after three months of storage (**B**).

ionic gelation method to prepare Cs NPs, Yilmaz et al. exploited the electrospray method to prepare essential oil-loaded Cs NPs, achieving a size of ~290 nm and a zeta potential of ~25.2 mV [51]. Table 5 summarizes the size and zeta potential of NPs related to formulation 11 and the mentioned studies.

To sum up, our described protocol details the key yet missing golden factors for easy and swift formulation of the optimized Cs NPs with nanosize (below 100 nm), proper zeta potential, homogeneity, good stability, and biocompatibility. These NPs can be used alone or as hybrid systems to envision a perfect encapsulation and delivery system for numerous pharmaceutical products and bioactive materials with applications in cancer therapy and other diseases.

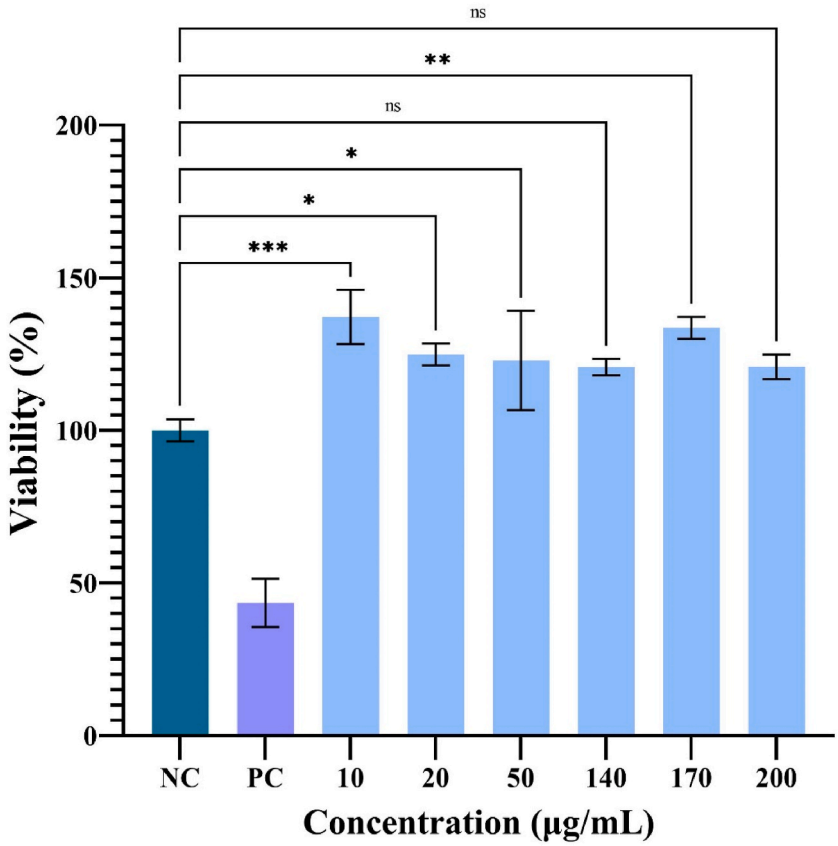

Fig. 8. Cell toxicity results for NIH-3T3 cells treated with different concentrations of Cs NPs. (ns: not significant: $P > 0.05$, *: $P < 0.05$, **: $P < 0.01$, ***: $P < 0.001$). NC: negative control, PC: positive control, ns: not significant.

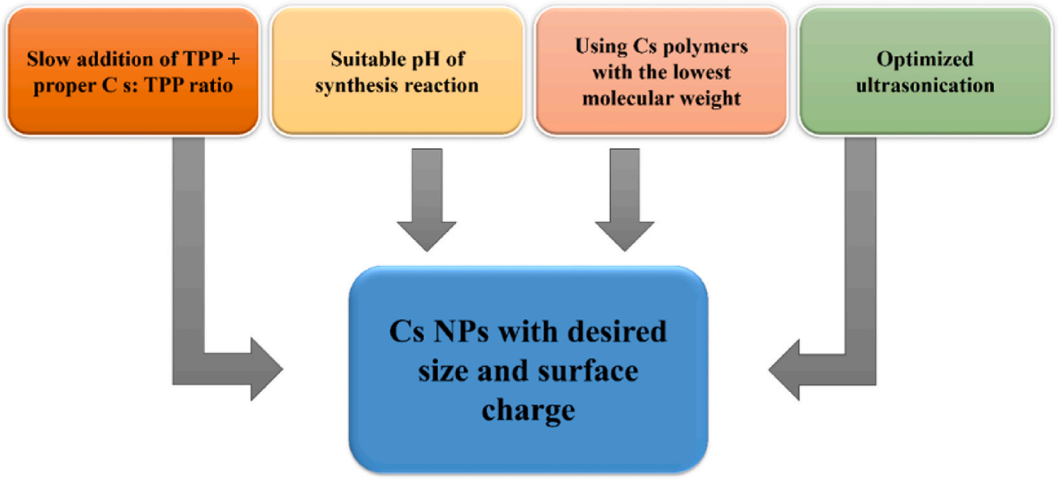

Fig. 9. The critical variables in the synthesis of Cs NPs with accepted size and surface charge.

4.4. The limitations of the study, suggestions, and prospective

While Cs NPs with desired properties can easily be prepared using the protocol of formulation 11, this study confronts some limitations. One of them is the *in vivo* investigation, which requires serious ethical considerations, high expenses, and is complex, which precluded this study from going forward to animal tests. On the other hand, one of the major concerns related to NPs is the

Table 5
Size and zeta potential related to formulation 11 and the other studies used Cs NPs, which have been noted.

Type of studied Cs NP	Size (nm)	Zeta potential (mV)	Ref
Formulation 11 of this study	~75.6	~26.7	_
Cs NPs	~290.3	~27.6	[47]
Cs NPs	~223.2	~34.5	[48]
zinc loaded Cs NPs	~387.7	~34.0	[49]
Cisplatin-loaded Cs NPs	~308.1	~30.5	[50]
Essential oil loaded Cs NPs	~290.0	~25.2	[51]

possibility of hazardous systemic harm, which requires *in vivo* studies. Meanwhile, this study highlights the high possibility of safe performance related to the optimized Cs NPs due to their favorable size and surface charge. Moreover, this research revealed another limitation, which is the decrease in probe ultrasonication outcome when the volume of sonicated suspension increases. Considering this point, this limitation may be addressed by performing a stronger and/or longer period of ultrasonication if the suspension volume is significantly high. Furthermore, although the presented methodology is claimed to be replicable, it is essential to acknowledge that discrepancies may arise in diverse laboratory conditions, equipment, and environmental variables.

Considering the reported data and outcomes, there are suggestions to be provided. In this study, NIH-3T3 cells were used to investigate the biocompatibility of optimized Cs NPs. In this regard, it is suggested to investigate this feature of Cs NPs on different normal cells to achieve a clearer vision about the non-toxicity of these NPs. Also, in subheading 4.3, the size and surface charge results of some studies that used Cs NPs were mentioned to compare the noted characteristics of the optimized Cs NPs in this study. To present a better comparison and understand the difference between the optimized Cs NPs of this research and other ones, a meta-analysis of the results of more studies could be beneficial.

In light of the remarkable discoveries made in this study, our forthcoming objectives encompass examining the influence of extended durations and varying storage conditions on the characteristics of the synthesized NPs, exploring the impact of diverse bioactive compounds and drugs encapsulated within the optimized Cs NPs on specific cancer types, and augmenting relevant *in vitro* experiments with *in vivo* examinations. Furthermore, while this study specifically examines the dimensions, electrical charge, structure, biocompatibility, and stability of the chosen formulation, it is crucial to explore additional factors such as the drug release rate, the effectiveness of drug loading, the efficiency of cellular uptake, biodistribution, pharmacokinetics, and actual therapeutic efficacy, which can differ depending on the specific compound being studied.

5. Conclusion

This article presents a novel method for creating Cs NPs with distinct physical and chemical properties. The emphasized approach is characterized by its rapidity and simplicity, ensuring a consistent and replicable synthesis process. Numerous factors have a substantial impact on the size and surface charge of NPs. These factors encompass the TPP:Cs ratio in the synthesis reaction, the gradual addition of the TPP solution to the Cs solution, the pH of the synthesis reaction, and the appropriate ultrasonication procedure. Additionally, the optimized NPs demonstrated stability for a period of three months, offering significant advantages for potential use in drug delivery and the formulation of pharmaceutical products. Likewise, these NPs demonstrated biocompatibility, along with their stability and the intended size (75.60 $\pm$ 18.24 nm) and zeta potential (26.70 $\pm$ 4.52 mV). Conclusively, the prepared Cs NPs and the method provided here serve as highly promising platform for drug delivery in diseases management.

Data availability

Data will be made available on request.

CRediT authorship contribution statement

Hamed Dadashi: Writing – original draft, Project administration, Investigation. **Somayeh Vandghanooni:** Writing – review & editing, Formal analysis. **Shahrbanoo Karamnejad-Faragheh:** Investigation. **Alireza Karimian-Shaddel:** Investigation. **Morteza Eskandani:** Writing – review & editing, Supervision, Conceptualization. **Rana Jahanban-Esfahlan:** Writing – review & editing, Supervision, Conceptualization.

Declaration of competing interest

None to declare.

Acknowledgement

The authors are grateful for financial support [grant number 68885] provided by Tabriz University of Medical Sciences, Tabriz, Iran.

References

[1] J.K. Patra, G. Das, L.F. Fraceto, E.V.R. Campos, MdP. Rodriguez-Torres, L.S. Acosta-Torres, et al., Nano based drug delivery systems: recent developments and future prospects, J. Nanobiotechnol. 16 (1) (2018) 71.
[2] P.G. Jamkhande, N.W. Ghule, A.H. Bamer, M.G. Kalaskar, Metal nanoparticles synthesis: an overview on methods of preparation, advantages and disadvantages, and applications, J. Drug Deliv. Sci. Technol. 53 (2019) 101174.
[3] H. Derakhshankhah, R. Jahanban-Esfahlan, S. Vandghanooni, S. Akbari-Nakhjavani, B. Massoumi, B. Haghshenas, et al., A bio-inspired gelatin-based pH- and thermal-sensitive magnetic hydrogel for in vitro chemo/hyperthermia treatment of breast cancer cells, J. Appl. Polym. Sci. 138 (n/a) (2021) 50578.
[4] A. Jafarizad, A. Taghizadehgh-Alehjougi, M. Eskandani, M. Hatamzadeh, M. Abbasian, R. Mohammad-Rezaei, et al., PEGylated graphene oxide/Fe3O4site: Synthesis, characterization, and evaluation of its performance as de novo drug delivery nanosystem, Bio Med. Mater. Eng. 29 (2) (2018) 177–190.
[5] S. Sargazi, S. Er, A. Mobashar, S.S. Gelen, A. Rahdar, N. Ebrahimi, et al., Aptamer-conjugated carbon-based nanomaterials for cancer and bacteria theranostics: a review, Chem. Biol. Interact. 361 (2022) 109964.
[6] H. Samadian, R. Mohammad-Rezaei, R. Jahanban-Esfahlan, B. Massoumi, M. Abbasian, A. Jafarizad, et al., A de novo theranostic nanomedicine composed of PEGylated graphene oxide and gold nanoparticles for cancer therapy, J. Mater. Res. 35 (4) (2020) 430–441.
[7] Z. Ranjbar-Navazi, Y. Omidi, M. Eskandani, S. Davaran, Cadmium-free quantum dot-based theranostics, TrAC, Trends Anal. Chem. 118 (2019) 386–400.
[8] M. Hashemi, A. Shamshiri, M. Saeedi, L. Tayebi, R. Yazdian-Robati, Aptamer-conjugated PLGA nanoparticles for delivery and imaging of cancer therapeutic drugs, Arch. Biochem. Biophys. 691 (2020) 108485.
[9] R. Jahanban-Esfahlan, B. Massoumi, M. Abbasian, A. Farnudiyan-Habibi, H. Samadian, A. Rezaei, et al., Dual stimuli-responsive polymeric hollow nanocapsules as “smart” drug delivery system against cancer, Polymer-Plastics Technology and Materials (2020) 1–13.
[10] B. Massoumi, M. Abbasian, R. Jahanban-Esfahlan, S. Motamedi, H. Samadian, A. Rezaei, et al., PEGylated hollow pH-responsive polymeric nanocapsules for controlled drug delivery, J Polymer International 69 (5) (2020) 519–527.
[11] B. Massoumi, M. Abbasian, R. Jahanban-Esfahlan, R. Mohammad-Rezaei, B. Khalilzadeh, H. Samadian, et al., A novel bio-inspired conductive, biocompatible, and adhesive terpolymer based on polyaniline, polydopamine, and polylactide as scaffolding biomaterial for tissue engineering application, Int. J. Biol. Macromol. 147 (2020) 1174–1184.
[12] M. Jaymand, R. Sarvari, P. Abbaszadeh, B. Massoumi, M. Eskandani, Y. Beygi-Khosrowshahi, Development of novel electrically conductive scaffold based on hyperbranched polyester and polythiophene for tissue engineering applications, Journal of Biomedical Materials Research - Part A 104 (11) (2016) 2673–2684.
[13] J.H. Ryu, H.Y. Yoon, I.C. Sun, I.C. Kwon, K. Kim, Tumor-targeting glycol chitosan nanoparticles for cancer heterogeneity, Adv. Mater. 32 (51) (2020) 2002197.
[14] B. Massoumi, M. Abbasian, B. Khalilzadeh, R. Jahanban-Esfahlan, H. Samadian, H. Derakhshankhah, et al., Electrically conductive nanofibers composed of chitosan-grafted polythiophene and poly (ε-caprolactone) as tissue engineering scaffold, Fibers Polym. 22 (1) (2021) 49–58.
[15] H. Mahmudi, M.A. Adili-Aghdam, M. Shahpouri, M. Jaymand, Z. Amoozgar, R. Jahanban-Esfahlan, Tumor microenvironment penetrating chitosan nanoparticles for elimination of cancer relapse and minimal residual disease, Front. Oncol. 12 (2022).
[16] K. Soleimani, E. Arkan, H. Derakhshankhah, B. Haghshenas, R. Jahanban-Esfahlan, M. Jaymand, A novel bioreducible and pH-responsive magnetic nanohydrogel based on β-cyclodextrin for chemo/hyperthermia therapy of cancer, Carbohydrate Polymers 252 (2021) 117229.
[17] Massoumi MA. Bakhshali, Balal Khalilzadeh, Rana Jahanban-Esfahlan, Aram Rezaei, Samadian HD. Hadi, Mehdi Jaymand, Gelatin-based nanofibrous electrically conductive scaffolds for tissue engineering applications, International Journal of Polymeric Materials and Polymeric Biomaterials (2020), https://doi.org/10.1080/00914037.2020.1760271.
[18] A. Jahanban-Esfahlan, A. Ostadrahimi, R. Jahanban-Esfahlan, L. Roufegarinejad, M. Tabibiazar, R. Amarowicz, Recent developments in the detection of bovine serum albumin, Int. J. Biol. Macromol. 138 (2019) 602–617.
[19] T.T.H. Thi, E.J. Suys, J.S. Lee, D.H. Nguyen, K.D. Park, N.P. Truong, Lipid-based nanoparticles in the clinic and clinical trials: from cancer nanomedicine to COVID-19 vaccines, Vaccines. 9 (4) (2021) 359.
[20] T.M. Allen, P.R. Cullis, Liposomal drug delivery systems: from concept to clinical applications, Adv. Drug Deliv. Rev. 65 (1) (2013) 36–48.
[21] H. Dianat-Moghadam, M. Heydarifard, R. Jahanban-Esfahlan, Y. Panahi, H. Hamishehkar, F. Pouremamali, et al., Cancer stem cells-emanated therapy resistance: implications for liposomal drug delivery systems, J Control Release 288 (2018) 62–83.
[22] A.A. Alsaad, A.A. Hussien, M.M. Gareeb, Solid lipid nanoparticles (SLN) as a novel drug delivery system: a theoretical review, Syst Rev Pharm 11 (2020) 259–273.
[23] F. Rasouliyan, M. Eskandani, M. Jaymand, Nakhjavani S. Akbari, R. Farahzadi, S. Vandghanooni, et al., Preparation, physicochemical characterization, and anti-proliferative properties of Lawsone-loaded solid lipid nanoparticles, Chem. Phys. Lipids 239 (2021).
[24] M. Zamanlu, M. Farhoudi, M. Eskandani, J. Mahmoudi, J. Barar, M. Rafi, et al., Recent advances in targeted delivery of tissue plasminogen activator for enhanced thrombolysis in ischaemic stroke, J. Drug Target. 26 (2) (2018) 95–109.
[25] Y.-P. Jia, B.-Y. Ma, X.-W. Wei, Z.-Y. Qian, The in vitro and in vivo toxicity of gold nanoparticles, Chin. Chem. Lett. 28 (4) (2017) 691–702.
[26] M. Niazi, E. Alizadeh, A. Zarebkohan, K. Seidi, M.H. Ayoubi-Joshaghani, M. Azizi, et al., Advanced bioresponsive multitasking hydrogels in the new era of biomedicine, Adv. Funct. Mater. 30 (45) (2021) 2104123.
[27] S. Hahn, D. Hennecke, What can we learn from biodegradation of natural polymers for regulation? Environ. Sci. Eur. 35 (1) (2023) 50.
[28] A. Grząbka-Zasadzińska, T. Amietszajew, S. Borysiak, Thermal and mechanical properties of chitosan nanocomposites with cellulose modified in ionic liquids, J. Therm. Anal. Calorimetry 130 (2017) 143–154.
[29] J. Yan, Z.-Y. Guan, W.-F. Zhu, L.-Y. Zhong, Z.-Q. Qiu, P.-F. Yue, et al., Preparation of puerarin chitosan oral nanoparticles by ionic gelation method and its related kinetics, Pharmaceutics 12 (3) (2020) 216.
[30] R. Jahanban-Esfahlan, H. Derakhshankhah, B. Haghshenas, B. Massoumi, M. Abbasian, M. Jaymand, A bio-inspired magnetic natural hydrogel containing gelatin and alginate as a drug delivery system for cancer chemotherapy, Int. J. Biol. Macromol. 156 (2020) 438–445.
[31] G. Kandasamy, R. Manisekaran, M.K. Arthikala, Chitosan nanoplatforms in agriculture for multi-potential applications - adsorption/removal, sustained release, sensing of pollutants & delivering their alternatives – a comprehensive review, Environ. Res. 240 (2024).
[32] N. Khatami, P. Guerrero, P. Martín, E. Quintela, V. Ramos, L. Saa, et al., Valorization of biological waste from insect-based food industry: assessment of chitin and chitosan potential, Carbohydrate Polymers 324 (2024).
[33] S. Abd El Wanees, M.G.A. Saleh, M.I. Alahmdi, N.H. Elsayed, M.M. Aljohani, M. Abdelfattah, et al., Benzotriazole-modified chitosan as a controller for the destruction of Al and H2 generation in the acidic environment, Mater. Chem. Phys. 311 (2024).
[34] L. Dong, Y. Li, H. Cong, B. Yu, Y. Shen, A review of chitosan in gene therapy: developments and challenges, Carbohydrate Polymers 324 (2024).
[35] P. Gupta, S. Sharma, S. Jabin, S. Jadoun, Chitosan nanocomposite for tissue engineering and regenerative medicine: a review, Int. J. Biol. Macromol. 254 (2024).
[36] J.P.M. Almeida, A.L. Chen, A. Foster, R. Drezek, In vivo biodistribution of nanoparticles, Nanomedicine. 6 (5) (2011) 815–835.
[37] X. Bai, S. Wang, X. Yan, H. Zhou, J. Zhan, S. Liu, et al., Regulation of cell uptake and cytotoxicity by nanoparticle core under the controlled shape, size, and surface chemistries, ACS Nano 14 (1) (2019) 289–302.
[38] M.P. Calatayud, B. Sanz, V. Raffa, C. Riggio, M.R. Ibarra, G.F. Goya, The effect of surface charge of functionalized Fe3O4 nanoparticles on protein adsorption and cell uptake, Biomaterials 35 (24) (2014) 6389–6399.
[39] H.H. Gustafson, D. Holt-Casper, D.W. Grainger, H. Ghandehari, Nanoparticle uptake: the phagocyte problem, Nano Today 10 (4) (2015) 487–510.
[40] R. Zein, W. Sharrouf, K. Selting, Physical properties of nanoparticles that result in improved cancer targeting, Journal of Oncology (2020) 2020.
[41] M. Eskandani, M. Eskandani, S. Vandghanooni, B. Navidshad, F.M. Aghjehgheshlagh, A. Nobakht, Protective effect of L-carnitine-loaded solid lipid nanoparticles against H2O2-induced genotoxicity and apoptosis, Colloids and Surfaces B: Biointerfaces. 212 (2022).
[42] S. Vandghanooni, F. Rasoulian, M. Eskandani, S. Akbari Nakhjavani, M. Eskandani, Acriflavine-loaded solid lipid nanoparticles: preparation, physicochemical characterization, and anti-proliferative properties, Pharmaceut. Dev. Technol. 26 (9) (2021) 934–942.

[43] M.B. Bahadori, S. Vandghanooni, L. Dinparast, M. Eskandani, S.A. Ayatollahi, A. Ata, et al., Triterpenoid corosolic acid attenuates HIF-1 stabilization upon cobalt (II) chloride-induced hypoxia in A549 human lung epithelial cancer cells, Fitoterapia 134 (2019) 493–500.
[44] H. Derakhshankhah, B. Haghshenas, M. Eskandani, R. Jahanban-Esfahlan, S. Abbasi-Maleki, M. Jaymand, Folate-conjugated thermal- and pH-responsive magnetic hydrogel as a drug delivery nano-system for "smart" chemo/hyperthermia therapy of solid tumors, Mater. Today Commun. 30 (2022) 103148.
[45] M. Azizi, R. Jahanban-Esfahlan, H. Samadian, M. Hamidi, K. Seidi, A. Dolatshahi-Pirouz, et al., Multifunctional nanostructures: intelligent design to overcome biological barriers, Materials Today Bio (2023) 100672.
[46] M. Shahpouri, M.A. Adili-Aghdam, H. Mahmudi, M. Jaymand, Z. Amoozgar, M. Akbari, et al., Prospects for hypoxia-based drug delivery platforms for the elimination of advanced metastatic tumors: from 3D modeling to clinical concepts, J. Contr. Release 353 (2023) 1002–1022.
[47] S.A. Fahmy, A. Ramzy, A.A. Mandour, S. Nasr, A. Abdelnaser, U. Bakowsky, et al., PEGylated chitosan nanoparticles encapsulating ascorbic acid and oxaliplatin exhibit dramatic apoptotic effects against breast cancer cells, Pharmaceutics 14 (2) (2022) 407.
[48] M. Hadidi, S. Pouramin, F. Adinepour, S. Haghani, S.M. Jafari, Chitosan nanoparticles loaded with clove essential oil: characterization, antioxidant and antibacterial activities, Carbohydrate polymers 236 (2020) 116075.
[49] R.C. Choudhary, R. Kumaraswamy, S. Kumari, S. Sharma, A. Pal, R. Raliya, et al., Zinc encapsulated chitosan nanoparticle to promote maize crop yield, Int. J. Biol. Macromol. 127 (2019) 126–135.
[50] M.H. Sultan, S.S. Moni, O.A. Madkhali, M.A. Bakkari, S. Alshahrani, S.S. Alqahtani, et al., Characterization of cisplatin-loaded chitosan nanoparticles and rituximab-linked surfaces as target-specific injectable nano-formulations for combating cancer, Sci. Rep. 12 (1) (2022) 468.
[51] M.T. Yilmaz, A. Yilmaz, P.K. Akman, F. Bozkurt, E. Dertli, A. Basahel, et al., Electrospraying method for fabrication of essential oil loaded-chitosan nanoparticle delivery systems characterized by molecular, thermal, morphological and antifungal properties, Innovat. Food Sci. Emerg. Technol. 52 (2019) 166–178.